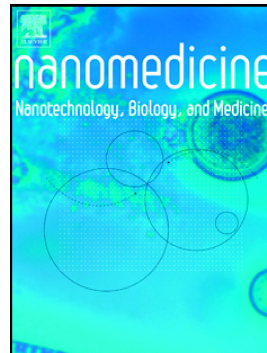


Accepted Manuscript

Tumor penetration of Sub-10nm nanoparticles: Effect of dendrimer properties on their penetration in multicellular tumor spheroids



Jason Bugno, Michael J. Poellmann, Karol Sokolowski, Hao-jui Hsu, Dong-Hwan Kim, Seungpyo Hong

PII: S1549-9634(19)30143-1

DOI: <https://doi.org/10.1016/j.nano.2019.102059>

Article Number: 102059

Reference: NANO 102059

To appear in: *Nanomedicine: Nanotechnology, Biology, and Medicine*

Revised date: 19 June 2019

Please cite this article as: J. Bugno, M.J. Poellmann, K. Sokolowski, et al., Tumor penetration of Sub-10nm nanoparticles: Effect of dendrimer properties on their penetration in multicellular tumor spheroids, *Nanomedicine: Nanotechnology, Biology, and Medicine*, <https://doi.org/10.1016/j.nano.2019.102059>

This is a PDF file of an unedited manuscript that has been accepted for publication. As a service to our customers we are providing this early version of the manuscript. The manuscript will undergo copyediting, typesetting, and review of the resulting proof before it is published in its final form. Please note that during the production process errors may be discovered which could affect the content, and all legal disclaimers that apply to the journal pertain.

Tumor Penetration of Sub-10 nm Nanoparticles: Effect of dendrimer properties on their penetration in multicellular tumor spheroids

Jason Bugno, Pharm.D., Ph.D.^{†,‡} Michael J. Poellmann, Ph.D.[†] Karol Sokolowski, B.S.[‡] Hao-jui Hsu, Ph.D.^{†,‡}, Dong-Hwan Kim, Ph.D.[§] and Seungpyo Hong, Ph.D.*^{†,‡,§,#}*

[†]Pharmaceutical Sciences Division, School of Pharmacy, University of Wisconsin, Madison, Wisconsin 53705, United States.

[‡]Department of Biopharmaceutical Sciences, University of Illinois at Chicago, Chicago, Illinois 60612, United States.

[§]School of Chemical Engineering, Sungkyunkwan University, Suwon, 16419, Republic of Korea.

*Yonsei Frontier Lab and Department of Pharmacy, Yonsei University, Seoul 03706, Republic of Korea.

*To Whom All Correspondence should be addressed:

Seungpyo Hong, Ph.D.

Professor

Division of Pharmaceutical Sciences

School of Pharmacy

The University of Wisconsin-Madison

777 Highland Ave.

Madison, WI 53705

seungpyo.hong@wisc.edu

Dong-Hwan Kim, Ph.D.

Professor

School of Chemical Engineering

Sungkyunkwan University

Seobu-ro 2066, Jangan-gu.

Suwon, Gyeonggi-do, 16419 South Korea

dhkim1@skku.edu

Word Count

Abstract: 146

Manuscript: 4,204

Number of References: 30

Number of Figures: 6

Acknowledgement

This study was supported by the National Science Foundation (NSF) under grant # DMR-1409161/1741560/1808251. The research was partially conducted in a facility constructed with support from the NIH (grant C06RR15482). J.B. received support in the form of fellowships from the American Association of Pharmaceutical Scientists (AAPS) and the American Foundation for Pharmaceutical Education (AFPE).

Abstract

Ulrasmall nanoparticles (NPs, <10 nm) have promise in cancer treatment, yet little is known about how NP physical properties influence penetration through solid tumors. To elucidate the role of NP size and structure, we prepared a series of sub-10 nm poly(amidoamine) (PAMAM) dendrimers and gold NPs (AuNP), and evaluated penetration in multicellular tumor spheroids (MCTS). Smaller generation 2 dendrimers (G2-NH₂, 2.9 nm diameter) penetrated 2.5-fold deeper than larger G7-NH₂ (8.1 nm) ($p = 0.0005$). Despite increased accumulation within MCTS, electrostatic cell interactions and ligand (folic acid, FA)-mediated targeting had minimal influence on penetration. NP rigidity played a minor role in penetration, with smaller rigid AuNP (2 nm) penetrating significantly more than larger AuNP (4 nm) (3-fold, $p = 0.014$; G2-NH₂ vs. G4-NH₂, 2.8-fold, $p = 0.033$). Our findings highlight the importance of rational NP design and provide design cues for tailored NP distributions within solid tumors.

KEYWORDS: Nanoparticles, dendrimer, cancer, tumor, penetration

Background

Nanoparticles (NPs) have been heavily investigated for their potential to deliver anticancer agents with controlled biodistributions, minimizing off-target effects and promoting efficacy.¹ Despite these promises, the vast majority of NP designs fail long before reaching the clinic. Over the past decade, relatively little improvement in NP delivery has been reported, suggesting a deeper understanding of NP-tumor interactions is required to accelerate their clinical translation.²

The characteristic tumor biology presents several barriers to efficient delivery.^{3,4} The rapid proliferation of tumor cells increases their distance ($>100\text{ }\mu\text{m}$) from the vasculature and causes local compressive forces on blood and lymphatic vessels. These phenomena generate nutrient gradients and subsequent changes in cell proliferation rates. As a result, cells at the tumor core are often found to be more resistant to agents that target rapidly proliferating cells.⁵ Furthermore, drug activity can be highly dependent on the metabolic environment and location of the target cells.⁶ It is thus necessary to develop a NP system that efficiently penetrates across the solid tumor. A promising engineering approach to achieve this would be controlling the tumor penetration behaviors of NPs through simple modification of their physical properties.

Not surprisingly, size matters. Larger sizes (100-200 nm) are typically associated with productive tumor accumulation via the enhanced permeability and retention (EPR) effect due to localized vascular leakage.⁷ However, they are too large to efficiently penetrate target tissues and are hindered by convective forces and high hydrostatic pressures within the tumor lymph. For this reason several groups have turned towards ultrasmall ($<10\text{ nm}$) particles in order to maintain efficient tumor penetration capabilities.⁵⁻⁷ Ultrasmall NPs ($<10\text{ nm}$) typically exhibit significantly enhanced tumor penetration properties compared to larger NPs.⁸⁻¹⁰ Within the sub-

10 nm size range, poly(amidoamine) (PAMAM) dendrimers provide an ideal platform for investigating the role NP properties play due to their precisely controllable size, near-monodispersity, and large number of surface terminal groups, allowing for facile multifunctionalization.^{11,12} Importantly, dendritic materials and PAMAM dendrimers have a substantial track record of tumor targeting for chemotherapy and gene delivery, theranostics, and imaging applications.¹³⁻¹⁶

The natural barriers to NP delivery and significant influence of NP physical properties on nano-bio interactions necessitate a better grasp on NP design parameters. Kannan, *et al.* have identified the need to engineer ‘critical nanoscale design parameters’ for optimizing NP pharmacokinetics and pharmacodynamics.¹⁷ This provides a strategy for linking physical parameters with *in vivo* limitations, and prioritizes a mechanistic understanding of how NP properties influence their tumor interactions.

We have previously identified that the penetration and accumulation of dendrimers within multicellular tumor spheroids (MCTS), a commonly used *in vitro* 3D solid tumor model, can be controlled by engineering their size and surface charge, respectively.¹⁰ Smaller, amine-terminated generation 2 PAMAM dendrimers (G2-NH₂, 2.9 nm as per manufacturer¹⁸) displayed significantly greater penetration properties than G4-NH₂ (4.5 nm) and G7-NH₂ (8.1 nm) (**Figure 1**). As shown in the fluorescence images of MCTS cryosections, G2-NH₂ was clearly observed within the extracellular space, whereas G7-NH₂ was diffusely distributed along the MCTS surface. These results led us to hypothesize that the transit pathway of dendrimers is dependent upon the dendrimer size, which is the underlying reason for their observed penetration differences.

Methods

Materials

PAMAM dendrimers were all purchased from Sigma Aldrich (St. Louis, MO). N-hydroxysuccinimide rhodamine (NHS-RHO) were obtained from Thermo Scientific (Rockford, IL). D,L-lactide was purchased from Polysciences Inc. (Warrington, PA). Cationic gold nanoparticles were purchased from Nanopartz (Loveland, CO). All other chemicals used in this study were purchased from Sigma Aldrich unless specified otherwise.

Microscopy and Image Analysis

All MCTS penetration was visualized using a Zeiss LSM 710 Meta confocal laser scanning microscope (CLSM, Carl Zeiss, Germany). The 543 nm line of a 1 mW tunable HeNe laser was used for the excitation of RHO, and emission was filtered at 565-595 nm. Images were captured using a 10x/0.25 Ph1 A-Plan objective. ImageJ was used for image analysis. For image analysis, whole MCTS were selected from brightfield images to generate a region of interest (ROI). The ROI was then overlaid over the corresponding fluorescence (FL) image. The ROI outer edge was made into a 1 pixel thick band and the average FL measured. The ROI was then shrunk by 1 pixel, a new band generated and the FL measured. This process was repeated to generate a profile of average FL vs. depth as measured by total pixels the ROI was shrunk. The surface of the MCTS thus corresponds to 0 pixel depth. Area under the curve (AUC) of the average FL vs. depth plot was used to describe the total accumulation of dendrimer within the entire MCTS. Penetration depth was measured based on average fluorescence at the innermost region of the MCTS core and applied evenly to all images within the experiment. Average fluorescence

intensity at the core of the MCTS was measured using ImageJ over an innermost area equal to one third the area of the entire MCTS.

Modeling Dendrimer Penetration into the MCTS

Dendrimer penetration was modeled based on our previously published data of dendrimer penetration in MCF-7 MCTS.⁹ All confocal intensity curves were normalized such that intensity was equal to '1' at the outer surface of the spheroid ($r = R$) and '0' as it approached the center. Fick's Second Law of diffusion is described by the following partial differential equation,

$$\frac{\partial c}{\partial t} = \nabla \cdot (D \nabla c) \quad (\text{Eq. 1})$$

where c was dendrimer concentration, t was time, and D described diffusivity. For one-dimensional, radial (r) transport in spherical coordinates, Eq. 1 became

$$\frac{\partial c}{\partial t} = \left[D^* \frac{\partial^2 c}{\partial r^2} + \frac{2D^*}{r} \frac{\partial c}{\partial r} \right] \quad (\text{Eq. 2})$$

where D^* was the effective diffusivity of the dendrimer within the MCTS. Because the concentration was measured indirectly as fluorescence intensity, we normalized each profile assuming an MCTS with radius (R) 0.3 mm, a concentration of 1 at $r = R$, and approaching a concentration of 0 from the outside-in. We then used Matlab (release R2017a, MathWorks, Natick, MA) to numerically solve the partial differential equation (function 'pdepe') described in Eq. 2. The initial condition was defined as

$$c(0 \leq r \leq R, t = 0) = 0 \quad (\text{Eq. 3})$$

and boundary conditions were defined as

$$\frac{\partial c}{\partial t} (r = 0, t) = 0 \quad (\text{Eq. 4})$$

$$c(r = R, t) = c_R \quad (\text{Eq. 5})$$

The parameters D^* , and c_R were identified by least squares fitting (default trust-region-reflective algorithm by the function ‘lsqcurvefit’) of a normalized distribution profile to the solution of the partial differential equation at time $t = t_{\text{treatment}}$. Only the monotonically decreasing section of each profile was fit with the model, shown in SI Figure 1-3.

Preparation of Surface Modified PAMAM Dendrimers

In order to visualize their interactions with biological systems, dendrimers were first labelled using NHS-rhodamine (RHO) and then surface modified as previously reported.¹⁰ For example, G2 PAMAM dendrimers were first purified using membrane dialysis against deionized distilled water (ddH₂O) and subsequently lyophilized. Purified G2 PAMAM dendrimer (40 mg, 12 μmol) was dissolved in 2 ml of ddH₂O. To this, NHS-RHO (7.8 mg, 14.7 μmol) in 300 μl DMSO was added dropwise with stirring. The reaction was carried out for 24 h at room temperature. Product was then purified by membrane dialysis against ddH₂O, or in the case of larger dendrimers, ultrafiltration (MWCO 3500 or 10000 kDa for G4 or G7 conjugates, respectively). Purified products were lyophilized, resulting in G2-RHO-NH₂ (G2-NH₂). RHO-labelled PAMAM dendrimers were also surface modified to contain acetylated surface groups. For instance, to acetylate the dendrimers, RHO-labelled G2 PAMAM dendrimers (13.5 mg, 3.6 μmol) were dissolved in 3 ml of methanol and reacted with acetic anhydride (29.1 mg, 285 μmol) and triethanolamine (36.1 mg, 357 μmol) for 24 h at room temperature, generating G2-RHO-Ac (G2-Ac). Acetylated materials were purified similar to their amine-terminated counterparts. Partially acetylated G5 PAMAM dendrimers were prepared similarly. G5 PAMAM was first RHO-labelled with NHS-RHO and purified by ultrafiltration (MWCO 3500 kDa) against ddH₂O. Partial acetylation was performed similarly to other dendrimer conjugates at 2.5%, 5%, 10%,

20%, 30%, 60%, 80%, and 100% molar ratios to the number of primary amines. Partially acetylated dendrimers were then purified as reported above. All prepared materials were characterized by ^1H NMR using a 400 MHz Bruker AV400 spectrometer (Bruker BioSpin Corp., Billerica, MA). Dendrimer zeta potential was measured in ddH₂O using dynamic light scattering with a Zetasizer Nano ZS (Malvern Instruments Inc., Westborough, MA).

Preparation of FA-Targeted PAMAM Dendrimers

FA-targeted, RHO-labelled, surface acetylated PAMAM dendrimers were prepared similar to that previously reported.⁸ In brief, FA (15.2 mg, 34.4 μmol) was activated in DMSO with excess EDC (66.0 mg, 344 μmol) and NHS (39.6 mg, 344 μmol), and the reaction let proceed at room temperature with stirring for 2 h. After 2 h, the appropriate amount of activated FA in DMSO was added dropwise to RHO-labelled amine-terminated dendrimers dissolved in DMSO. A 2-, 6-, and 15-fold molar excess of FA to dendrimer reaction ratio was used for reactions with G2, G4, and G7 dendrimers, respectively. RHO-labelled, FA-conjugated dendrimers were purified by repetitive dialysis against ddH₂O and lyophilized. Resulting dendrimer conjugates were next dissolved in methanol and surface acetylated with excess acetic anhydride (4-fold molar excess to surface amines), and purified by repetitive dialysis or ultrafiltration against ddH₂O as described above. All prepared materials were characterized by ^1H NMR using a 400 MHz Bruker AV400 spectrometer (Bruker BioSpin Corp., Billerica, MA).

Preparation of AuNPs

In order to prepare gold nanoparticles (AuNP) similar in size to G2 and G4 PAMAM dendrimers, RHO-labelled cationic AuNP either 2.2 nm or 4 nm were prepared, termed AuNP (G2) or AuNP (G4), respectively. AuNPs were dissolved in ddH₂O at 2.5 mg/mL (38 μM AuNP (G2) or 6.5

μM AuNP (G4), 0.36 mL). To this, NHS-RHO (3-fold excess to AuNP (G2) or 6-fold excess to AuNP (G4)) dissolved in minimal DMSO was added dropwise. The reaction was let proceed at room temperature overnight with stirring. Product was purified by ultrafiltration (MWCO 3 kDa) against ddH₂O, and resulting product solution was stored at 4°C prior to use.

Cell Culture

The KB cell line was purchased from the American Type Tissue Collection (ATCC, Manassas, VA) and grown continuously as a monolayer at 37°C, 5% CO₂ in folate-deficient GIBCO RPMI 1640 medium (Invitrogen Corporation, Carlsbad, CA) supplemented with penicillin (100 units/ml) and 10% heat-inactivated fetal bovine serum (FBS) (Invitrogen). The MCF-7 cell line was graciously donated by the Tonetti lab at the University of Illinois at Chicago and grown continuously as a monolayer at 37°C, 5% CO₂ in DMEM medium (Mediatech, Inc., Manassas, VA) supplemented with penicillin (100 units/ml) and 10% heat-inactivated FBS.

Penetration Assay Using Multicellular Tumor Spheroids (MCTS)

MCTS were prepared using the liquid overlay method. For example, KB cells from a confluent T-75 KB cells from a confluent T-75 flask were detached using trypsin-EDTA and resuspended in supplemented RPMI 1640 medium at a concentration of 10,000 cells/ml. Two hundred microliters of cell suspension were added to each well of a 96-well plate coated with 50 μL of 1.5% agarose in RPMI 1640. The cells were incubated on agarose for 5 d to allow the formation of MCTS. MCF-7 MCTS were prepared similarly using supplemented DMEM medium and a seeding concentration of 12,000 cells/mL.

For evaluating the penetration of partially acetylated G5 dendrimers in MCF-7 MCTS after 5 d to allow for growth of the MCTS, 100 μL of media was removed and replaced with 100 μL of

fluorescence normalized 2X dendrimer stocks in supplemented DMEM, and treated for the desired timepoints prior to confocal imaging. Final G5 dendrimer concentration ranged from approximately 100-200 nM.

For evaluating the penetration of G2-NH₂, G4-NH₂, and G7-NH₂ in the presence of endocytosis inhibitors MCF-7 MCTS were allowed to first form for 5 d as described above. Concentrations of endocytosis inhibitors was as follows: 2.1 μ g/mL chlorpromazine, 1.0 μ g/mL filipin, 1.5 μ g/mL cytochalasin D, or 1 mg/mL sodium azide and 8.2 mg/mL deoxyglucose in combination. For treatment, 100 μ L was removed from each well, and 100 μ L of 2X inhibitor added. This pretreatment was run for 30 min. After 30 min, 100 μ L was removed from each well and 100 μ L of 1X inhibitor and fluorescence normalized 2X dendrimer stock in supplemented DMEM was added and the treatment let run for either 5, 12, or 24 h. Final dendrimer concentrations were approximately 60 nM G7-NH₂, 244 nM G4-NH₂, or 1.3 μ M G2-NH₂.

For evaluating the penetration of AuNPs, all materials were fluorescence normalized and MCTS were treated as described for the experiments above. Final concentrations for G2-RHO-NH₂ and G4-RHO-NH₂ were approximately 19.2 μ M and 2.4 μ M, respectively.

2D cell culture was performed similarly to the MCTS assays using 96 well tissue culture plates. Cells were treated for the desired timepoints, the media removed, and the cells washed three times using PBS. Images were taken with an Olympus IX70 inverted microscope (Olympus Scientific Solutions America Corp., Waltham, MA) using QCapture Pro software (QImaging, Surrey, BC, Canada).

Statistical Analysis

For evaluating the penetration of partially acetylated G5 PAMAM dendrimers and dendrimers in the presence of various endocytosis inhibitors results are reported as the mean and standard error from at least $n = 5$ replicates from the same cell passage, and is consistent with multiple independent experiments of separate passages. All other experiments, unless otherwise noted, represent mean measurements and standard error from $n = 3$ separate cell passages. Statistical significance was determined using 2-way ANOVA followed by Tukey's post-hoc analysis of multiple comparisons with alpha = 0.05 using GraphPad Prism version 7.00 for Windows, GraphPad Software, La Jolla California USA.

Results

Modeling Penetration through the Tumor

In this study, we first hypothesized that if G2-NH₂ freely diffused the extracellular space, its penetration profile would follow Fick's Second Law of Diffusion.¹⁹ In contrast, larger dendrimers unable to rapidly penetrate paracellular, or penetrating via a transcellular route, would exhibit slower penetration, as they are dependent on the kinetics of repeating cycles of endocytosis, cellular transit, and subsequent exocytosis. We prepared a mathematical model based on Fick's Second Law of Diffusion solved with boundary conditions and simulated diffusion within a sphere to derive values of relative diffusivity by nonlinear least squares fitting (Eq. 1). The model was fit to our previously published findings of dendrimer penetration in MCF-7 MCTS (**Figure 2**).¹⁰ G2-NH₂ profiles from 0.5 to 24 h were described partially by the diffusion model (SI Figure 1 and SI Table 1), although the apparent diffusivity decreased with time. In contrast, simple diffusion did not describe the penetration profiles of either larger G4-NH₂ (SI Figure 2) or G7-NH₂ dendrimers (SI Figure 3). Notably, diffusivity values derived at each time point did not scale with the inverse of NP radius, as would be the case for a freely diffusing spherical particle according to the Stokes-Einstein relation (**Figure 2B** and **2C**). These findings support our hypothesis that transport of PAMAM dendrimers, larger G4-NH₂ and G7-NH₂ in particular, is driven by one or more non-diffusive phenomena.

Influence of Charge-Mediated Cellular Interactions on Tumor Penetration

We next postulated that the difference in penetration route could, at least in part, be affected by the level of dendrimer-cell interactions, and less likely due to the relatively small differences in dendrimer size.^{20, 21} Thus, our second hypothesis was that G7-NH₂, with more

cationic surface groups (512 vs. 16 of G2-NH₂), interacted strong enough with cell membranes to delay their transit beyond the first few cell layers. Conversely, G2-NH₂ may elicit enough charge-based cellular interactions to accumulate within the MCTS, yet not so much as to delay penetration. To better assess this hypothesis, we examined the effect of dendrimer-cell interactions and uptake on penetration using two methods: partial surface charge neutralization of dendrimers and use of chemical inhibitors of cellular uptake.

We prepared a series of dendrimers with various degrees of surface charge to examine the influence of charge-mediated cellular interactions on penetration. G5 PAMAM dendrimers (5.4 nm) were employed as they are just slightly larger than the apparent penetration size cutoff between G2-NH₂ and G4-NH₂, and contain twice as many of the surface groups (128) as G4-NH₂ (64), allowing us to evaluate a large range of surface charge. Zero, 2.5, 5, 10, 20, 30, 60, or 100% surface neutralization was accomplished via acetylation (SI Figures 4 and 5). If charge-mediated cellular interactions hinder the penetration of higher generation dendrimers, improved penetration with acetylation would be expectedly observed. Surprisingly, surface neutralization did not enhance dendrimer penetration (**Figure 3** and SI Figure 6). PAMAM dendrimers with higher acetylation degrees (i.e. 60-100%) demonstrated the poorest penetration characteristics (**Figure 3B**). This difference can be likely attributed to the significantly lower surface accumulation of neutral dendrimer compared to positively charged ones (**Figure 3A and 3C**). Overall MCTS surface accumulation of dendrimers within the MCTS, and in 2D cell culture were inversely proportional to the degree of acetylation (SI Figure 7). These results suggest the surface charge of PAMAM dendrimers does not noticeably affect their penetration into cellular masses, although it plays a key role in determining the level of cell interactions.

Impact of Cellular Uptake on Tumor Penetration

We then investigated if the cellular uptake of dendrimers affects their penetration within MCTS. MCF-7 MCTS were treated with G2-NH₂, G4-NH₂, or G7-NH₂ in the presence of various endocytosis inhibitors, and their penetration behaviors were evaluated (**Figure 4**). PAMAM dendrimers have been shown to internalize into cells via multiple pathways.¹¹ Endocytosis has been reported to be inhibited by either chlorpromazine (clathrin-mediated), filipin (caveolae-mediated), cytochalasin D (macropinocytosis), or both sodium azide and deoxyglucose (energy dependent via ATP depletion).²²⁻²⁷ We speculated that if larger dendrimers transited the MCTS via a transcellular pathway, decreasing the cellular uptake would enhance the penetration of dendrimers, which would be more pronounced in the case of larger ones. Interestingly, G4-NH₂ and G7-NH₂ penetration was unaffected by treatment with any of the endocytosis inhibitors (**Figure 4B** and SI Figure 9). Cytochalasin D, an inhibitor of macropinocytosis, had a penetration enhancement effect on G2-NH₂ at a time point as early as 5 h, with significantly greater penetration after 12 h compared to MCTS not treated with endocytosis inhibitors (4.3-fold, $p < 0.0005$). A similar enhancement in G2-NH₂ penetration was observed following filipin treatment after 12 h (3.25-fold, $p = 0.059$). However, by 24 h, all G2-NH₂ showed enhanced penetration into the MCTS, with the exception of those treated with chlorpromazine. Nonetheless, G2-NH₂ was still able to penetrate the innermost regions of the MCTS even in the presence of chlorpromazine, as observed on images (**Figure 4A**). The limited penetration based on image quantification is likely due to poor surface accumulation of G2-NH₂ in the presence of chlorpromazine.

Effect of NP Rigidity on Tumor Penetration

The distinct penetration difference between G2-NH₂ and G4-NH₂ implies a size cutoff for rapid transit between 2.9-4.5 nm. These findings suggest that the cellular uptake of larger dendrimers does not significantly contribute to their retention within the MCTS periphery, disproving our second hypothesis. Instead, our results support that the small differences in dendrimer size may in fact dictate their penetration kinetics. We were intrigued by the fact that a relatively small size (< 3 nm) difference between G2-NH₂ and G4-NH₂ was sufficient to lead to notably different penetration profiles. However, it seemed possible that this effect may be specific to the flexible nature of smaller dendrimers, considering that larger dendrimers may form chain entanglement, decreasing their conformational flexibility. To examine the effect of NP flexibility and composition, the MCTS penetration behaviors of G2-NH₂ and G4-NH₂ dendrimers were compared with similarly sized, positively charged, rigid 2 nm and 4 nm gold NPs (AuNP), respectively. AuNPs have been investigated for their potential as imaging agents and for therapeutic delivery to cancers.^{9,28,29} Interestingly, AuNPs demonstrated similar penetration trends as those of their comparatively sized dendrimer counterparts (**Figure 5**). Within 6 h, G2-NH₂ exhibited a 2.8-fold enhancement in penetration depth compared to G4-NH₂ ($p = 0.033$). A similar 3.1-fold enhanced penetration was observed between AuNP (2 nm) and AuNP (4 nm) ($p = 0.014$). Both G4-NH₂ and AuNP (4 nm) exhibited notably greater surface binding, followed by poor penetration into the MCTS compared to either of their smaller counterparts (**Figure 5B**). These results provide further evidence that the penetration of ultrasmall NPs within MCF-7 MCTS is likely due to the small size difference between the NPs, irrespective of particle composition or flexibility.

Tumor Penetration of Ligand-Targeted NPs

Lastly, we examined the effect of targeting ligands conjugated to the dendrimer surface on the tumor penetration. Ligand-mediated targeting is a commonly used strategy for accumulating NPs at the tumor site in a specific manner through specific ligand-receptor interactions.^{1, 30, 31} Folic acid (FA) was employed for this study as a model molecule as it is a commonly used targeting ligand for dendrimers to target FA receptors (FAR) overexpressed on a variety of cancers.^{8, 32} FA was conjugated to G2, G4, and G7 PAMAM dendrimers, followed by full acetylation, and their penetration in KB MCTS overexpressing the FAR was evaluated (**Figure 6** and SI Figure 10). FA-targeted dendrimers exhibited markedly greater accumulation in the MCTS compared to nontargeted dendrimers (**Figure 6A** and **6E**). By 24 h, G2-FA and G4-FA demonstrated remarkably enhanced accumulation compared to their nontargeted counterparts (207-fold, $p = 0.005$ and 58.7-fold, $p = 0.002$, respectively). Moreover, targeted dendrimers also penetrated the KB MCTS in a size-dependent manner. Within as little as 1 h, G2-FA penetrated greater than any other group (**Figure 6A** and **6B**). Penetration of G4-FA lagged behind G2-FA, yet by 24 h of treatment reached a similar accumulation within the innermost regions of the MCTS (**Figure 6D**). G7-FA exhibited the slowest penetration kinetics within the MCTS, being mostly retained within the outer regions of the MCTS after 24 h. Taken together, these findings further demonstrated that the penetration of ligand-targeted dendrimers is size dependent.

Discussion

Our findings indicate that NP size is the major determinant of tumor penetration. Interestingly, surface charge, cellular uptake, and the conjugation of targeting ligands did not play as significant of a role in the penetration behaviors. However, we found that overall accumulation of NPs within the MCTS was determined by the surface characteristics. That is, positively charged dendrimers exhibited significantly greater MCTS accumulation, an effect likely mediated through interactions with negatively charged constituents of the cell membrane. This phenomena has been well documented in conventional 2D cell culture.^{20,21} Similarly, cell-specific interactions mediated via FA resulted in as much as 200-fold accumulation enhancements.

Among all of our experiments herein, NPs less than 3 nm more rapidly penetrated the MCTS compared to those larger than 4 nm. Even among NPs with differing compositions (dendrimers vs. AuNPs), the penetration behaviors of the NPs smaller than 3 nm were more similar to each other than to their larger counterparts. These findings suggest a possible size threshold (~3 nm) for penetration, which could be potentially universally applicable to many NP systems. Future experiments will be required to identify biological factors that contribute to this observed threshold. It is likely that a combination of cell junctions and matrix proteins would influence NP penetration into the solid tumor.^{7,33} For instance, Wang *et al.* have identified that the junction protein desmoglein-2 can hinder the distribution of AuNPs within solid tumors.³⁴ Similarly, collagenase-coating NPs can lead to a 4-fold enhancement in NP penetration through degradation of components of the tumor extracellular matrix.³⁵

While PAMAM dendrimers are well-known for their precise size and surface characteristics, it is important to note that polydispersities among materials exist and could

contribute to our findings. For instance, van Dongen and coauthors have demonstrated that while commercially available G5 PAMAM dendrimers are composed of approximately 65% G5 dendrimers, they are a heterogeneous mixture, including smaller components and larger tetramers.³⁶ We attempted to minimize smaller impurities through ultrafiltration, yet larger sizes will be included in final materials. It should be noted that previous analysis of commercial samples from the vendor used resulted in polydispersity (PDI) values ranging from 1.01-1.04.³⁷,³⁸ AuNPs obtained from Nanopartz came with a certificate of analysis including NP size, as measured by transmission electron microscopy (TEM). AuNP (2 nm) and AuNP (4 nm) had sizes and percent polydispersities of 2.2 nm and 4 nm, and 20% and 10%, respectively.

In conclusion, this study provides design cues for tailoring the tumor penetration and intratumoral distribution of ultrasmall NPs by controlling their physical properties (most effectively by size). While additional information is needed for elucidating the barrier to efficient NP penetration at sizes larger than only several nanometers, our results demonstrate that physical parameter optimization is necessary for achieving desired distributions of NPs within the solid tumor, which is itself critical for optimal anticancer drug effects.

Figure Legends

Figure 1. Unique penetration pathways of various generation (differently sized) PAMAM dendrimers. Cryosections of tumor spheroids suggest differences in extracellular/intracellular ratio among the dendrimers. We propose that G2-NH₂ (labeled with rhodamine) is able to rapidly penetrate the MCTS via a paracellular pathway, in which transit is largely diffusion mediated. In contrast, penetration of larger dendrimers, such as G7-NH₂, is limited as they are either too large to penetrate efficiently through the extracellular space, or transit via a slower transcellular pathway.

Figure 2. Modeling dendrimer penetration in MCF-7 MCTS. (A) Penetration of RHO-labelled PAMAM dendrimers within MCF-7 MCTS. (B) Normalized diffusivity and (C) diffusivity relative to G2-NH₂, plotted against the inverse of the nominal NP radius R. If transport was governed only by diffusion, diffusivity would be linear with respect to 1/R according to the Stokes-Einstein equation. Scale bar is 200 μ m. Panel (A) was adapted in part with permission from Bugno, J.; Hsu, H.-J.; Pearson, R. M.; Noh, H.; Hong, S., Size and Surface Charge of Engineered Poly(amidoamine) Dendrimers Modulate Tumor Accumulation and Penetration: A Model Study Using Multicellular Tumor Spheroids. *Mol. Pharmaceutics* 2016, 13 (7), 2155-2163. Copyright 2019 American Chemical Society.

Figure 3. Effect of charge-based cellular interactions on dendrimer penetration. (A) MCF-7 MCTS were treated with partially acetylated G5 PAMAM dendrimers ranging from 0-100% surface neutralization. (B) Partial surface acetylation did not enhance dendrimer MCTS penetration. (C) Surface neutralization was associated with notably lower dendrimer accumulation within the MCTS. Scale bar is 500 μ m.

Figure 4. Influence of cellular uptake on dendrimer penetration in MCF-7 MCTS. (A)

Penetration of PAMAM dendrimers in the presence of various endocytosis inhibitors. (B)

Inhibition of cellular uptake did not enhance penetration of G4-NH₂ or G7-NH₂. In contrast, within 12 h G2-NH₂ penetration was enhanced in the presence of inhibitors of caveolae (filipin) and macropinocytosis (cytochalasin D) mediated endocytosis. Scale bar is 500 μ m. * p = 0.059, ** p < 0.0005

Figure 5. MCTS interactions of flexible PAMAM dendrimers and their similarly-sized rigid AuNPs counterparts. (A) Penetration depth of PAMAM dendrimers and AuNPs. (B) Cross-sectional fluorescence profiles at 24 h indicate different penetration characteristics of smaller G2-NH₂ and AuNP (2 nm) compared with their larger counterparts G4-NH₂ and AuNP (4 nm). A depth of 0 pixels corresponds to the MCTS surface. * p < 0.05

Figure 6. Interactions of neutral folic acid (FA)-targeted dendrimers with FAR-overexpressing KB MCTS. (A) Confocal images of KB MCTS treated with neutral acetylated (-Ac) FA-targeted and nontargeted dendrimers. Whereas FA-targeted dendrimers rapidly accumulated within the MCTS, nontargeted dendrimers did not penetrate the MCTS as indicated by the absence of signal within the MCTS. (B-D) Cross-sectional profiles of FA-targeted dendrimer penetration into the MCTS at various time points. (E) Total accumulation of dendrimers within the MCTS. Scale bar is 200 μ m.

References

1. Peer, D.; Karp, J. M.; Hong, S.; Farokhzad, O. C.; Margalit, R.; Langer, R., Nanocarriers as an emerging platform for cancer therapy. *Nat. Nanotechnol.* **2007**, *2* (12), 751-760.
2. Wilhelm, S.; Tavares, A. J.; Dai, Q.; Ohta, S.; Audet, J.; Dvorak, H. F.; Chan, W. C. W., Analysis of nanoparticle delivery to tumours. *Nat. Rev. Mater.* **2016**, *1*, 16014.
3. Pearson, R. M.; Hsu, H.-j.; Bugno, J.; Hong, S., Understanding nano-bio interactions to improve nanocarriers for drug delivery. *MRS Bull.* **2014**, *39* (3), 227-237.
4. Minchinton, A. I.; Tannock, I. F., Drug penetration in solid tumours. *Nat. Rev. Cancer* **2006**, *6* (8), 583-592.
5. West, G. W.; Weichselbaum, R.; Little, J. B., Limited Penetration of Methotrexate into Human Osteosarcoma Spheroids as a Proposed Model for Solid Tumor Resistance to Adjuvant Chemotherapy. *Cancer Res.* **1980**, *40* (10), 3665-3668.
6. Teicher, B. A.; Lazo, J. S.; Sartorelli, A. C., Classification of Antineoplastic Agents by their Selective Toxicities toward Oxygenated and Hypoxic Tumor Cells. *Cancer Res.* **1981**, *41* (1), 73-81.
7. Jain, R. K.; Stylianopoulos, T., Delivering nanomedicine to solid tumors. *Nat. Rev. Clin. Oncol.* **2010**, *7* (11), 653-64.
8. Sunoqrot, S.; Bugno, J.; Lantvit, D.; Burdette, J. E.; Hong, S., Prolonged blood circulation and enhanced tumor accumulation of folate-targeted dendrimer-polymer hybrid nanoparticles. *J. Control. Release* **2014**, *191*, 115-22.
9. Huang, K.; Ma, H.; Liu, J.; Huo, S.; Kumar, A.; Wei, T.; Zhang, X.; Jin, S.; Gan, Y.; Wang, P. C.; He, S.; Zhang, X.; Liang, X.-J., Size-Dependent Localization and

Penetration of Ultrasmall Gold Nanoparticles in Cancer Cells, Multicellular Spheroids, and Tumors in Vivo. *ACS Nano* **2012**, *6* (5), 4483-4493.

10. Bugno, J.; Hsu, H.-J.; Pearson, R. M.; Noh, H.; Hong, S., Size and Surface Charge of Engineered Poly(amidoamine) Dendrimers Modulate Tumor Accumulation and Penetration: A Model Study Using Multicellular Tumor Spheroids. *Mol. Pharmaceutics* **2016**, *13* (7), 2155-2163.
11. Bugno, J.; Hsu, H.-j.; Hong, S., Recent advances in targeted drug delivery approaches using dendritic polymers. *Biomater. Sci.* **2015**, *3* (7), 1025-1034.
12. Bugno, J.; Hsu, H.-j.; Hong, S., Tweaking dendrimers and dendritic nanoparticles for controlled nano-bio interactions: potential nanocarriers for improved cancer targeting. *J. Drug Targeting* **2015**, *23* (7-8), 642-650.
13. Liu, J.; Xiong, Z.; Zhang, J.; Peng, C.; Klajnert-Maculewicz, B.; Shen, M.; Shi, X., Zwitterionic Gadolinium(III)-Complexed Dendrimer-Entrapped Gold Nanoparticles for Enhanced Computed Tomography/Magnetic Resonance Imaging of Lung Cancer Metastasis. *ACS Appl. Mater. Interfaces* **2019**, *11* (17), 15212-15221.
14. Fan, Y.; Zhang, J.; Shi, M.; Li, D.; Lu, C.; Cao, X.; Peng, C.; Mignani, S.; Majoral, J.-P.; Shi, X., Poly(amidoamine) Dendrimer-Coordinated Copper(II) Complexes as a Theranostic Nanoplatform for the Radiotherapy-Enhanced Magnetic Resonance Imaging and Chemotherapy of Tumors and Tumor Metastasis. *Nano Lett.* **2019**, *19* (2), 1216-1226.
15. Xiong, Z.; Shen, M.; Shi, X., Dendrimer-based strategies for cancer therapy: Recent advances and future perspectives. *Sci. China Mater.* **2018**, *61* (11), 1387-1403.
16. Fan, Y.; Sun, W.; Shi, X., Design and Biomedical Applications of Poly(amidoamine)-Dendrimer-Based Hybrid Nanoarchitectures. *Small Methods* **2017**, *1* (12), 1700224.

17. Kannan, R. M.; Nance, E.; Kannan, S.; Tomalia, D. A., Emerging concepts in dendrimer-based nanomedicine: from design principles to clinical applications. *J. Intern. Med.* **2014**, *276* (6), 579-617.
18. In <http://dendritech.com/pamam.html>; Dendritech, I. M., MI.
19. Tang, B. C.; Dawson, M.; Lai, S. K.; Wang, Y.-Y.; Suk, J. S.; Yang, M.; Zeitlin, P.; Boyle, M. P.; Fu, J.; Hanes, J., Biodegradable polymer nanoparticles that rapidly penetrate the human mucus barrier. *Proc. Natl. Acad. Sci. U. S. A.* **2009**, *106* (46), 19268-19273.
20. Hong, S.; Bielinska, A. U.; Mecke, A.; Keszler, B.; Beals, J. L.; Shi, X.; Balogh, L.; Orr, B. G.; Baker, J. R., Jr.; Banaszak Holl, M. M., Interaction of poly(amidoamine) dendrimers with supported lipid bilayers and cells: hole formation and the relation to transport. *Bioconjugate Chem.* **2004**, *15* (4), 774-82.
21. Hong, S.; Leroueil, P. R.; Janus, E. K.; Peters, J. L.; Kober, M.-M.; Islam, M. T.; Orr, B. G.; Baker, J. R.; Banaszak Holl, M. M., Interaction of Polycationic Polymers with Supported Lipid Bilayers and Cells: Nanoscale Hole Formation and Enhanced Membrane Permeability. *Bioconjugate Chem.* **2006**, *17* (3), 728-734.
22. New, E. J.; Parker, D., The mechanism of cell uptake for luminescent lanthanide optical probes: the role of macropinocytosis and the effect of enhanced membrane permeability on compartmentalisation. *Org. Biomol. Chem.* **2009**, *7* (5), 851-855.
23. Shen, J.; He, Q.; Gao, Y.; Shi, J.; Li, Y., Mesoporous silica nanoparticles loading doxorubicin reverse multidrug resistance: performance and mechanism. *Nanoscale* **2011**, *3* (10), 4314-4322.

24. Zeng, X.; Zhang, Y.; Nyström, A. M., Endocytic Uptake and Intracellular Trafficking of Bis-MPA-Based Hyperbranched Copolymer Micelles in Breast Cancer Cells. *Biomacromolecules* **2012**, *13* (11), 3814-3822.

25. Wei, Z.; Yuan, S.; Hao, J.; Fang, X., Mechanism of inhibition of P-glycoprotein mediated efflux by Pluronic P123/F127 block copolymers: Relationship between copolymer concentration and inhibitory activity. *Eur. J. Pharm. Biopharm.* **2013**, *83* (2), 266-274.

26. Chavanpatil, M. D.; Khdair, A.; Gerard, B.; Bachmeier, C.; Miller, D. W.; Shekhar, M. P. V.; Panyam, J., Surfactant–Polymer Nanoparticles Overcome P-Glycoprotein-Mediated Drug Efflux. *Mol. Pharmaceutics* **2007**, *4* (5), 730-738.

27. Miura, S.; Suzuki, H.; Bae, Y. H., A multilayered cell culture model for transport study in solid tumors: Evaluation of tissue penetration of polyethyleneimine based cationic micelles. *Nano Today* **2014**, *9* (6), 695-704.

28. Kumar, A.; Ma, H.; Zhang, X.; Huang, K.; Jin, S.; Liu, J.; Wei, T.; Cao, W.; Zou, G.; Liang, X.-J., Gold nanoparticles functionalized with therapeutic and targeted peptides for cancer treatment. *Biomaterials* **2012**, *33* (4), 1180-1189.

29. Zhang, X.; Chibli, H.; Mielke, R.; Nadeau, J., Ultrasmall Gold–Doxorubicin Conjugates Rapidly Kill Apoptosis-Resistant Cancer Cells. *Bioconjugate Chem.* **2011**, *22* (2), 235-243.

30. Jiang, X.; Bugno, J.; Hu, C.; Yang, Y.; Herold, T.; Qi, J.; Chen, P.; Gurbuxani, S.; Arnovitz, S.; Strong, J.; Ferchen, K.; Ulrich, B.; Weng, H.; Wang, Y.; Huang, H.; Li, S.; Neilly, M. B.; Larson, R. A.; Le Beau, M. M.; Bohlander, S. K.; Jin, J.; Li, Z.; Bradner, J. E.; Hong, S.; Chen, J., Eradication of Acute Myeloid Leukemia with FLT3 Ligand–Targeted miR-150 Nanoparticles. *Cancer Res.* **2016**, *76* (15), 4470-4480.

31. Modi, D. A.; Sunoqrot, S.; Bugno, J.; Lantvit, D. D.; Hong, S.; Burdette, J. E., Targeting of follicle stimulating hormone peptide-conjugated dendrimers to ovarian cancer cells. *Nanoscale* **2014**, *6* (5), 2812-2820.

32. Kukowska-Latallo, J. F.; Candido, K. A.; Cao, Z.; Nigavekar, S. S.; Majoros, I. J.; Thomas, T. P.; Balogh, L. P.; Khan, M. K.; Baker, J. R., Nanoparticle Targeting of Anticancer Drug Improves Therapeutic Response in Animal Model of Human Epithelial Cancer. *Cancer Res.* **2005**, *65* (12), 5317-5324.

33. Jain, R. K., Transport of Molecules in the Tumor Interstitium: A Review. *Cancer Res.* **1987**, *47* (12), 3039-3051.

34. Wang, C. E.; Yumul, R. C.; Lin, J.; Cheng, Y.; Lieber, A.; Pun, S. H., Junction opener protein increases nanoparticle accumulation in solid tumors. *J. Control. Release* **2018**, *272*, 9-16.

35. Goodman, T. T.; Olive, P. L.; Pun, S. H., Increased nanoparticle penetration in collagenase-treated multicellular spheroids. *Int. J. Nanomed.* **2007**, *2* (2), 265-74.

36. van Dongen, M. A.; Orr, B. G.; Banaszak Holl, M. M., Diffusion NMR Study of Generation-Five PAMAM Dendrimer Materials. *J. Phys. Chem. B* **2014**, *118* (25), 7195-7202.

37. Uppuluri, S.; Dvornic, P. R.; Tan, N. C. B.; Hagnauer, G., The Properties of Dendritic Polymers 2: Generation Dependence of the Physical Properties of Poly(amidoamine) Dendrimers. *Army Research Laboratory* **1999**, *ARL-TR-1774*.

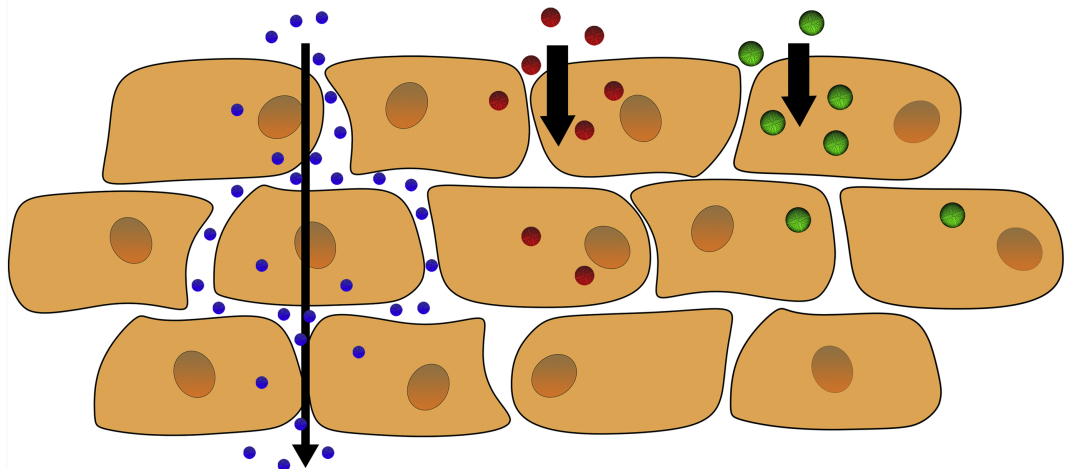
38. Mullen, D. G.; Desai, A.; van Dongen, M. A.; Barash, M.; Baker, J. R., Jr.; Banaszak Holl, M. M., Best practices for purification and characterization of PAMAM dendrimer. *Macromolecules* **2012**, *45* (12), 5316-5320.

Graphical Abstract

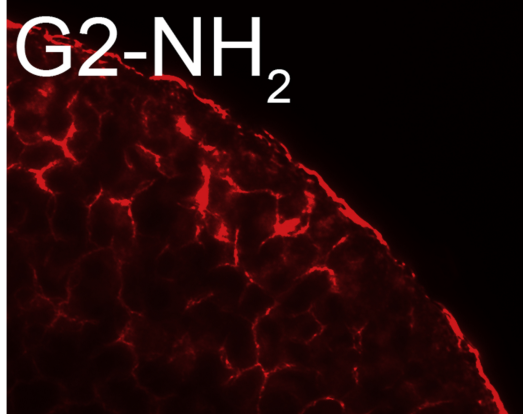
Little is known regarding how nanoparticle (NP) physical properties influence tumor penetration.

In a tumor model we evaluated sub-10 nm poly(amidoamine) dendrimers and gold NP penetration. Penetration was strictly size-dependent, within minimal influence of electrostatic interactions, ligand targeting, cellular uptake, and rigidity. We provide insights for tailored NP tumor distributions.

G2 G4 G7



G2-NH₂



G7-NH₂

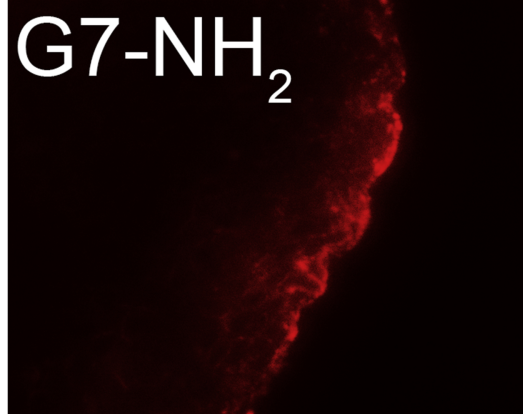
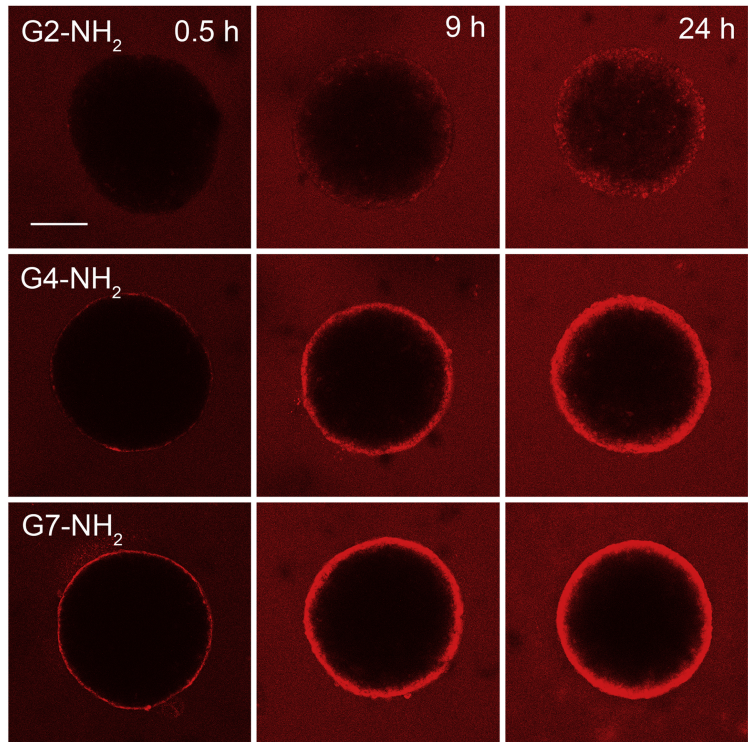
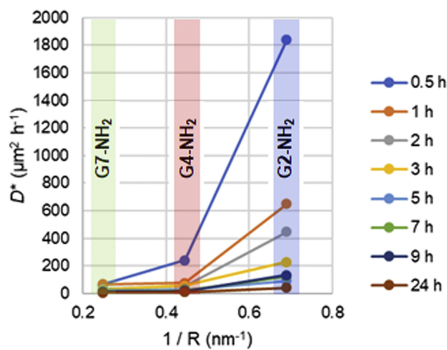


Figure 1

A



B



C

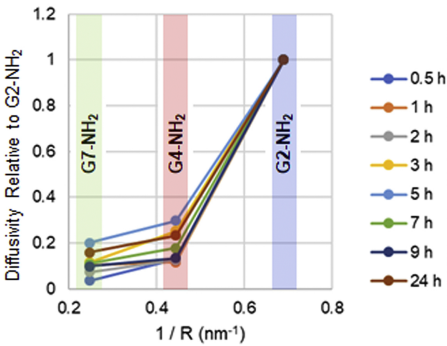


Figure 2

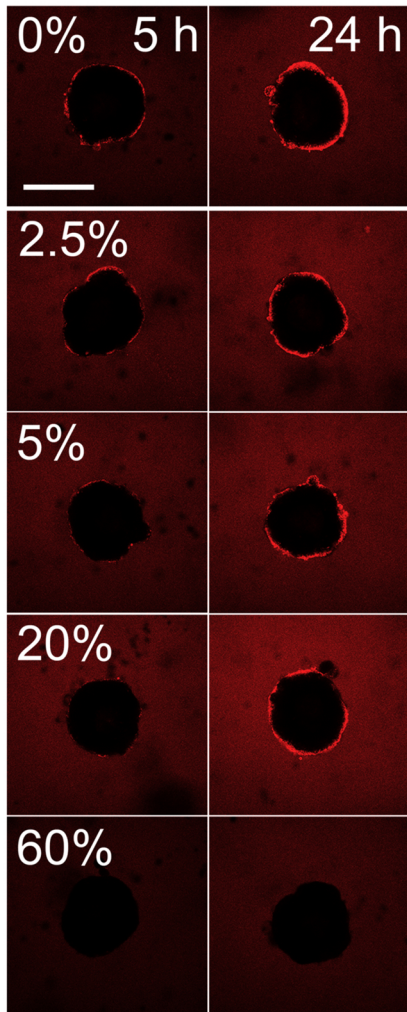
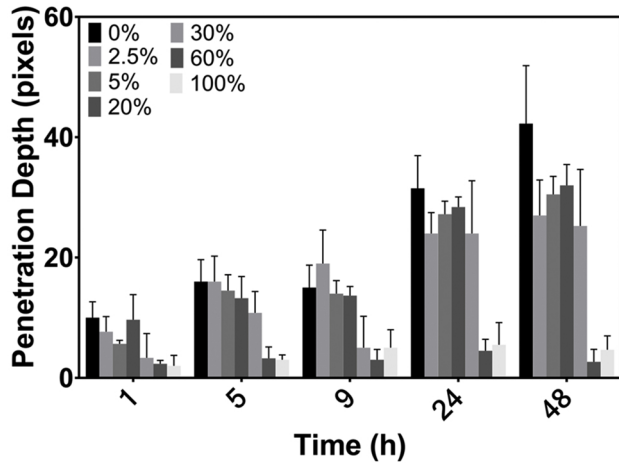
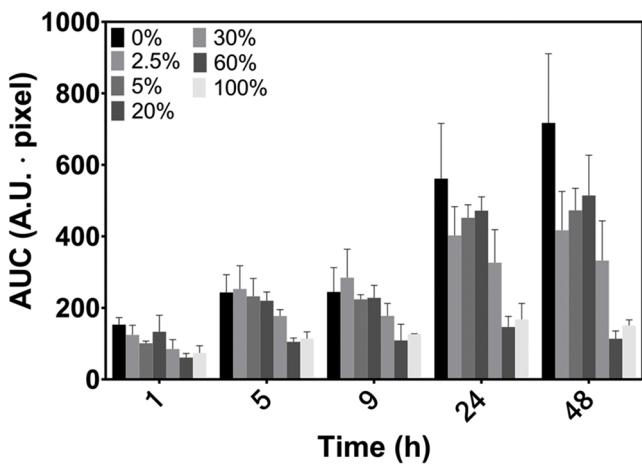
A**B****C**

Figure 3

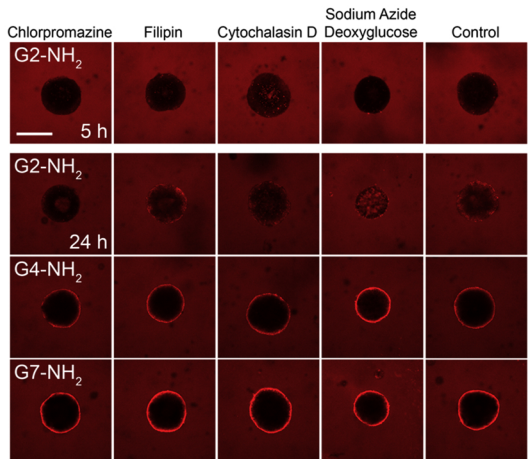
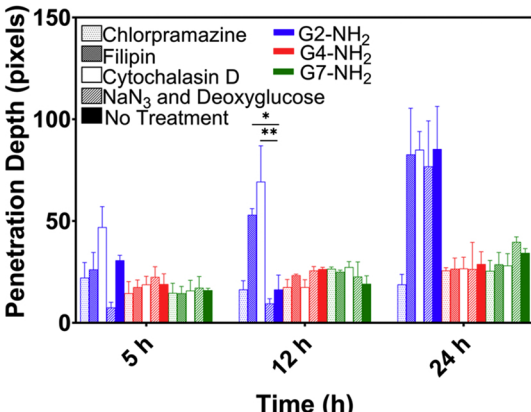
A**B**

Figure 4

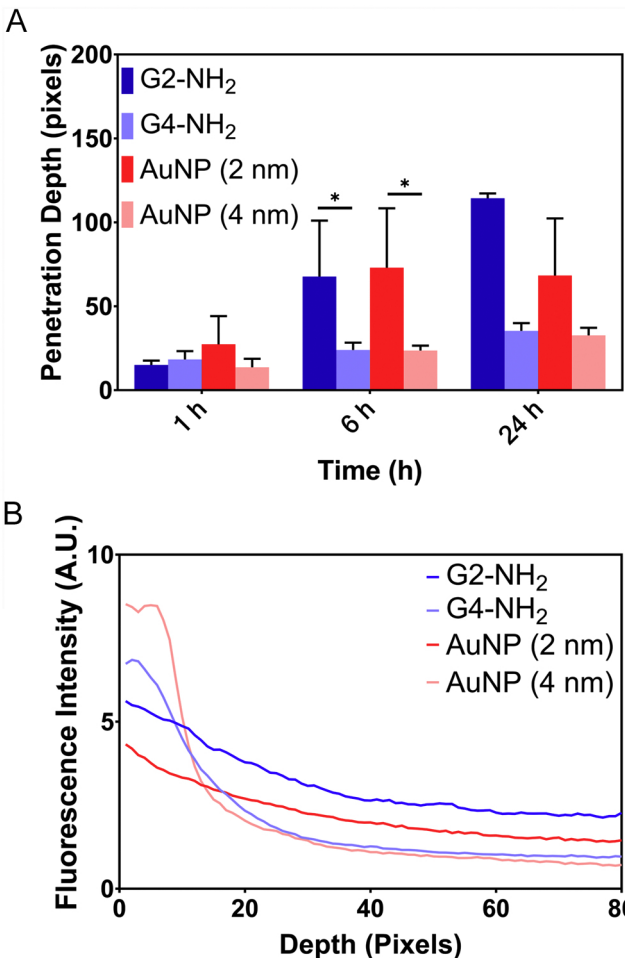
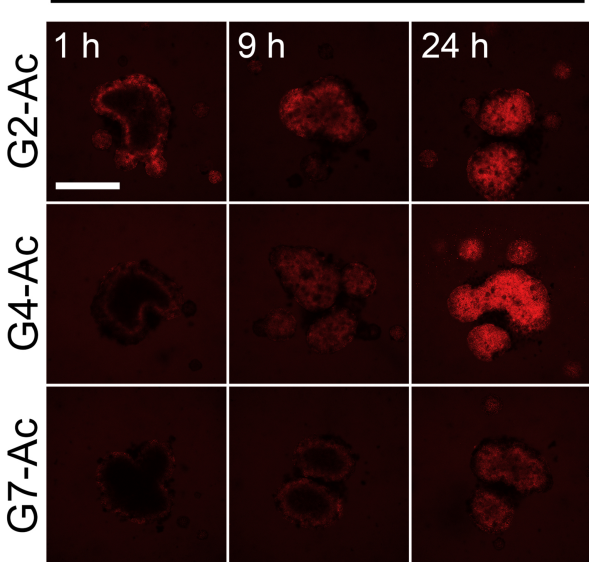
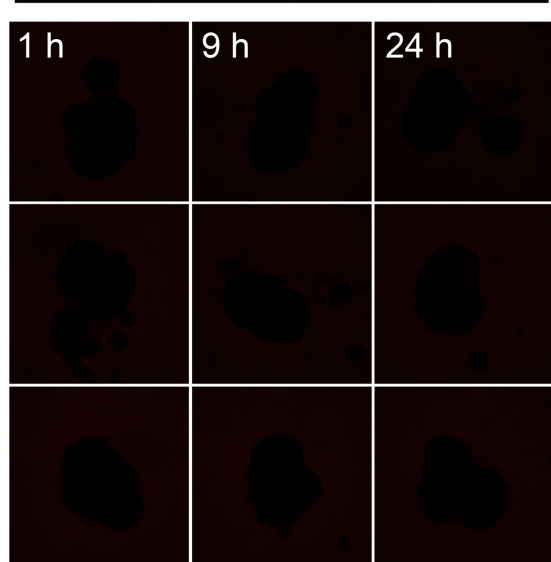


Figure 5

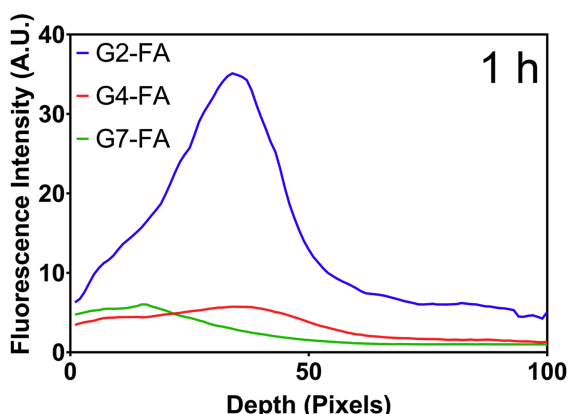
A Folate-Targeted



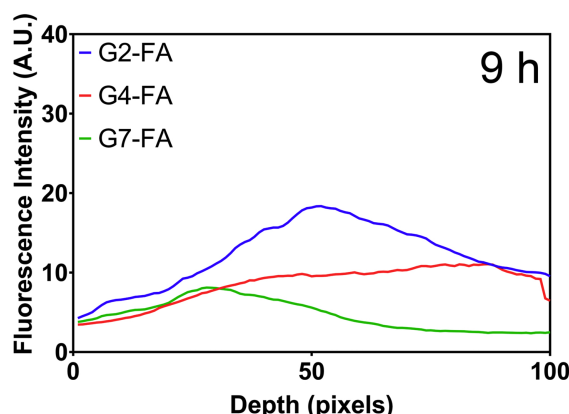
No Targeting



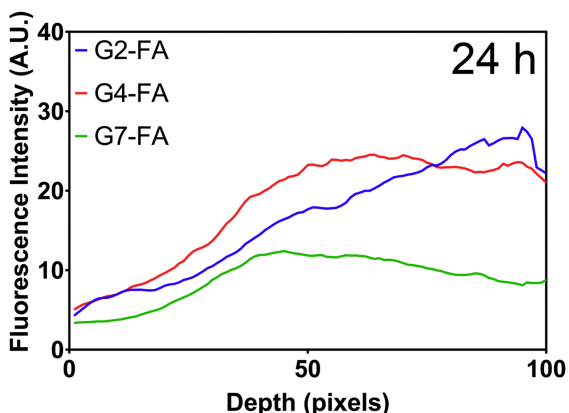
B



C



D



E

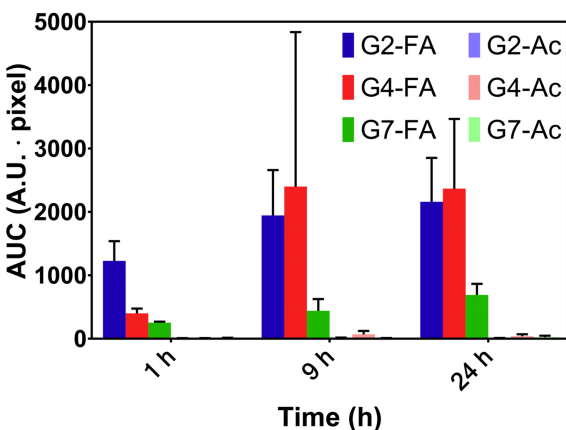


Figure 6